JOURNAL OF SOLID STATE CHEMISTRY 136, 274–283 (1998)
ARTICLE NO. SC977706

Wet Chemical Synthesis of Sr- and Mg-Doped $LaGaO_3$, a Perovskite-Type Oxide-Ion Conductor

Keqin Huang and John B. Goodenough

Center for Materials Science and Engineering, ETC 9.102, The University of Texas at Austin, Austin, Texas 78712

Received August 12, 1997; in revised form November 10, 1997; accepted November 18, 1997

Sr- and Mg-doped $LaGaO_3$ ultrafine powders were prepared by a sol–gel process that involves an acetate solution of the cations followed by ammonia peptization. The formed gel precursor consists of a hydrous complex of hydroxo and acetate ligands with the cations. Dehydration occurs when the gel is heated, and the complex of hydroxo and acetate ligands with the cations precipitates. Thermal analysis (DTA/TGA) reveals endothermic peaks corresponding to the decomposition of the hydroxo ligand at 220°C and the acetate ligand at 280°C followed by a strong exothermic peak at 330°C; gases are liberated by the cleavage of the CH_3COO^- ligands. The coupling of the endothermic peak at 280°C and the exothermic peak at 330°C is found to be a characteristic phenomenon for the breakup of the CH_3COO^- bond. The IR spectroscopy of products at different stages of decomposition further confirms the existence of OH^- and CH_3COO^- ligands and the assumptions about chemical reactions made in this study. TEM observations show an average 50-nm particle size after calcination at 500°C. The X-ray diffraction patterns indicate a single perovskite cubic phase after sintering at 1400°C, yielding a 94% dense sample. Hydrothermal treatment of the gel and the Pechini method were also used for comparison.

Key Words: **lanthanum gallate; sol–gel; oxide-ion conductor; solid oxide fuel cell; precursor.**

1. INTRODUCTION

Sr- and Mg-doped $LaGaO_3$ (LSGM) has been found to be an excellent oxide-ion conductor over a broad range of oxygen partial pressures ($1–10^{-22}$ atm) at low temperatures (1–7). It promises to replace commercially available oxide-ion conductors such as Y_2O_3–ZrO_2 for use in a reduced-temperature solid oxide fuel cell (7). However, a commercial solid oxide fuel cell requires a thin-film electrolyte with a high area/thickness ratio to reduce the energy loss when a current passes through it. Thin-film fabrication technologies, such as tape-casting and calendar-casting, require submicron powders to produce a high-quality ceramic membrane. Conventional ceramic techniques are unable to provide LSGM powders with particle sizes less than 1 micron. We have therefore been motivated to make ultrafine powders by another synthetic routine.

Wet chemical syntheses of oxide powders that are precipitated from a homogeneous aqueous solution of cation ingredients have been reported. These methods mainly include the sol–gel process, coprecipitation, and hydrothermal reactions. The sol–gel process is an attractive route that starts from molecular precursors and forms an oxide network via inorganic polymerization reactions. It promises to offer many advantages, including high purity, ultrahomogeneity, and reduction of the sintering temperature required for materials processing.

Hydrothermal synthesis is an aqueous ceramic process that uses hot pressurized water for precipitation of anhydrous, well-crystallized ceramic powders (8–10). Since the hydrothermal reaction replaces the calcination required by sol–gel and coprecipitation processes, this technique is able to produce agglomerate-free ceramic powders.

The Pechini method (11), or liquid-mixing method (12–14), calls for forming a chelate between mixed cations (dissolved as salts such as nitrates or chlorides in an aqueous solution) and a hydroxycarboxylic acid (citric acid is preferred). Mixing with a polyhydroxy alcohol such as ethylene glycol or diethylene glycol at medium temperature produces a polyesterification; finally, a solid polymer resin is formed that is cross-linked and homogeneous.

In this paper we report the synthesis of Sr- and Mg-doped $LaGaO_3$ via a sol–gel, the Pechini method, and hydrothermal reactions. The powders thus obtained were characterized by X-ray diffraction, thermal analysis, transmission electron microscopy (TEM), and Fourier transform infrared spectroscopy (FTIR spectroscopy). The reaction mechanisms are discussed.

2. EXPERIMENTAL PROCEDURE

2.1. Synthesis of Precursors, and Intermediate and Final Products

For all three methods used in this study, stock salt solutions containing the cation ingredients are preferred over

0022-4596/98 $25.00

TABLE 1
Concentrations of the Stock Solutions Used in This Study

	Solution						
	$La(CH_3COO)_3$	$Sr(CH_3COO)_2$	$Mg(CH_3COO)_2$	$La(NO_3)_3$	$Sr(NO_3)_2$	$Ga(NO_3)_3$	$Mg(NO_3)_2$
g of oxide/ml of solution	0.0170	0.1029	0.2145	0.04741	0.1058	0.04917	0.1282

solid salts. These stock solutions include the acetates $La(CH_3COO)_3$, $Sr(CH_3COO)_2$, and $Mg(CH_3COO)_2$ and the nitrates $La(NO_3)_3$, $Sr(NO_3)_2$, $Ga(NO_3)_3$, and $Mg(NO_3)_2$. The concentrations of each solution used in this study are given in Table 1; they were standardized by weighing a 5-ml solution before and after it was heated.

The sol–gel synthesis of doped $LaGaO_3$ perovskite via acetates of the components has been reported previously (3). The stoichiometric amounts of each component acetate solution (gallium nitrate used instead of gallium acetate) for yielding 10 g of final product $La_{0.8}Sr_{0.2}Ga_{0.83}Mg_{0.17}O_{2.815}$ (LSGM) were intimately mixed by stirring in a 1000-ml beaker; 20 ml of ammonia solution with 30% concentration was then slowly added to the above solution to form a white gel at around pH 10.0. The resulting gel was then aged at room temperature for at least 3 days and evaporated in a constant-temperature oven instead of on a thermal plate, a procedure that was later proved necessary to yield better powders. The evaporating rate of the gel was carefully controlled by adjusting the amount of mixed solution and heating temperatures. A possible chemical reaction, sensitive to the temperature during the evaporation of the gel, destroys the gel and forms precipitates (see later discussion). In this study, we selected 150°C for 8 hr to complete the dehydration and drying. For comparison, the resulting product was decomposed at 300, 500, and 700°C for various times, and at each stage, the product was further characterized by X-ray diffraction, thermal analysis, and IR spectroscopy.

By the Pechini method, the required amounts of nitrate solutions were mixed at room temperature. A calculated amount of citric acid was added to the solution: 1 mol of trivalent cation needs 1 mol of citric acid and 1 mol of divalent cation needs 2/3 mol of citric acid. For this study, about 1.5 times the amount of citric acid consumed by the final product is necessary to complete the chelate reaction. After 30 min of stirring, approximately the same molar amount of ethylene glycol as citric acid was added to the chelated solution; the solution was then heated to 150°C to allow the chelates to undergo polyesterification as well as to remove excess water. This process usually takes overnight and finally results in a solid polymeric "resin". The resin obtained was charred by slowly heating to about 300°C; it was further calcined at 1000°C for 8 hr to form crystallites of the mixed-oxide composition. A subsequent 6-hr ball-milling in a polyethylene jar containing ZrO_2 beads in ethanol is needed to break up the soft agglomerates.

For the hydrothermal treatment, a gel formed in the sol–gel process was used as the precursor of the hydrothermal reactions. The Teflon cup (23 ml) of a 4745 Parr bomb filled with the gel and its mother liquor (pH $\sim$10.0) was placed in a stainless-steel vessel. The bomb was then heated in an oven for 2–10 hr at 200°C and finally quenched to room temperature. The resulting products were washed with deionized water and ethanol to remove any anionic impurities and desiccated in an oven at 150°C overnight. The dried product was then characterized by X-ray diffraction, thermal analysis, TEM, and IR spectroscopy.

2.2. Thermal Analysis

The decomposition of the intermediate products was monitored with a Perkin-Elmer DTA 1700 and TGA 7 thermal analyzer in an oxidizing atmosphere (N_2 + 21% O_2, flow rate 100 ml/min). Unlike most thermal analyses, the DTA/TGA runs conducted in this study were carried out separately from room temperature to 700 or 900°C at a rate of 10°C/min.

2.3. IR Spectroscopy

IR spectra were recorded at room temperature with a Nicolet Magna-550 spectrometer, which has a resolution of about 2.5 cm^{-1}. Thin, transparent pellets were made by compacting an intimate mixture obtained by shaking 1 mg of the sample in 100 mg of KBr.

2.4. Particle Characterization

The particle size and morphology of the LSGM powders prepared were examined by TEM with a JEOL JEM-200CX microscope. The powders were first dispersed into methanol in an ultrasonic cleaner (Cole-Parmer 8851) for 20 min; the suspended solution was then dropped on a carbon-coated copper grid with a pipette, and the copper grid was then fixed onto the sample holder of the microscope.

BET surface areas of the prepared powders were measured with a Micromeritics ASAP 2010 surface area analyzer. The powders were carefully degassed before the measurement.

2.5. Sintering of the Powders

After calcination, powders were pressed into pellets and sintered from 1350 to 1400°C for various times. X-ray diffraction with Ni-filtered Cu$K\alpha$ radiation was used to monitor the phase evolution in the samples. The density of the sintered ceramic was measured with a Micromeritics AccuPyc 1330 pycnometer.

3. RESULTS AND DISCUSSION

3.1. Description of the Reactions

The sol–gel process is usually very sensitive to experimental parameters such as temperature, pH, chemical composition, concentration of the reactants, and nature of the solvent. The first step, after dissolving the acetate salts in water, consists of forming mixed aquo complexes of La^{3+}, Sr^{2+}, Ga^{3+}, and Mg^{2+}, as illustrated for La^{3+} in the following:

$$La^{3+} + O\begin{matrix}H\\H\end{matrix} \longrightarrow \left[La\text{---}O\begin{matrix}H\\H\end{matrix}\right]^{3+}$$

aquo complex

$$\longrightarrow [La\text{---}OH]^{2+} + H^{+}. \qquad [1]$$

hydroxo complex

This complexation reaction at room temperature and pH 3.5 occurs easily according to the specific coordination requirements of the lanthanide ions.

Considering the high oxygen coordination numbers of La^{3+} (CN = 12) and Ga^{3+} (CN = 6), mixed nucleophilic-ligand systems such as OH^- and CH_3COO^- may provide strong complexation with probably a predominant electrostatic attraction in the aqueous solution (15).

In the following ammonia peptizing stage, it is expected that several chemical reactions could take place, such as inter- and intramolecular rearrangements or conversion of aquo-bridged species to hydroxo–aquo complexes. However, the anions CH_3COO^- and OH^- play a decisive role in the homogeneous condensation of the solution. In most cases they are strongly coordinated to cations and thus end up in the precipitates where they affect the particle morphology of the final products. In most simple cases, an associated species such as $[La(OH)_2(CH_3COO)(OH_2)_9]$, which was confirmed by later TGA measurement, can be formed where both positively charged hydrolyzed cations $[La(OH)_2(OH_2)_9]^+$ and negatively charged anions, e.g., CH_3COO^-, are simultaneously present in an aqueous solution. Such M–X associations have been clearly shown by optical spectroscopy (16, 17), NMR (18, 19), or X-ray scattering (20, 21). The full coordination of cations such as La^{3+} in the hydroxo–aquo precursor is already satisfied. The coordination of an anionic species like CH_3COO^- with such a precursor occurs via a nucleophilic substitution. Since CH_3COO^- (electronegativity 2.24) is less electronegative than the H_2O ligands (electronegativity 2.49), electrons are transferred from CH_3COO^- to the precursor. The negative charge of the CH_3COO^- decreases, giving rise to a more covalent M–CH_3COO^- bond, which is not dissociated by the solvent. Thus complexes such as $[La(OH)_2(CH_3COO)(OH_2)_9]$ are the natural product. In contrast, NO_3^- is hard to associate with cations such as La^{3+} since NO_3^- is more electronegative (electronegativity 2.76) than H_2O; electrons are attracted by NO_3^-, and the overall electron transfer goes from precursor to NO_3^-, which increases the negative charge of NO_3^- and makes the M–NO_3^- bond more ionic. As a result, the high dielectric constant of the aqueous solvent favors ion formation and makes the association of NO_3^- with cation M difficult. In this stage, the intermediate products are hydrated, amorphous gelatinous precipitates as observed in the experiment with a pH value of around 10. A sufficient aging time at room temperature is found to be necessary for completion of the foregoing complexation reactions.

Raising the gel temperature in the following evaporation process breaks up the aquo ligands in the hydroxo–aquo complexes and precipitates related associated species such as $La(OH)_2(CH_3COO)$ or $Ga(OH_2)(CH_3COO)$. LaO(CH_3COO) or GaO(CH_3COO) may be alternative precipitates. After several hours of evaporation, the pH of the clear solution above the precipitates becomes neutral (pH 7), which further confirms the assumed reaction route. On the other hand, the formation of CH_3COONH_4 also self-buffers the solution at a pH value of 6.5–7.0. At the end point of the evaporation, therefore, the resulting products are the complex of the hydroxides and acetates with the cations as is also demonstrated by the thermal analysis and IR results (see Section 3.3). This process can be illustrated by

$$La^{3+} + 2OH^- + CH_3COO^- + 9H_2O$$
$$\xrightarrow{\text{complexing}} La(OH)_2(CH_3COO)(OH_2)_9$$
$$\xrightarrow{\text{heating}} La(OH)_2(CH_3COO)\downarrow + 9H_2O. \qquad [2]$$

The phase evolution of the precursor with calcine temperature is shown in Fig. 1. The intermediate products from 300 to 700°C are multiphase, including mainly the perovskite phase, La_2O_3, $LaSrGa_3O_7$, and $La_2O_2CO_3$. Raising the temperature to 1400°C enhances the cation diffusion, and a single cubic phase is formed as pointed out in ref 5.

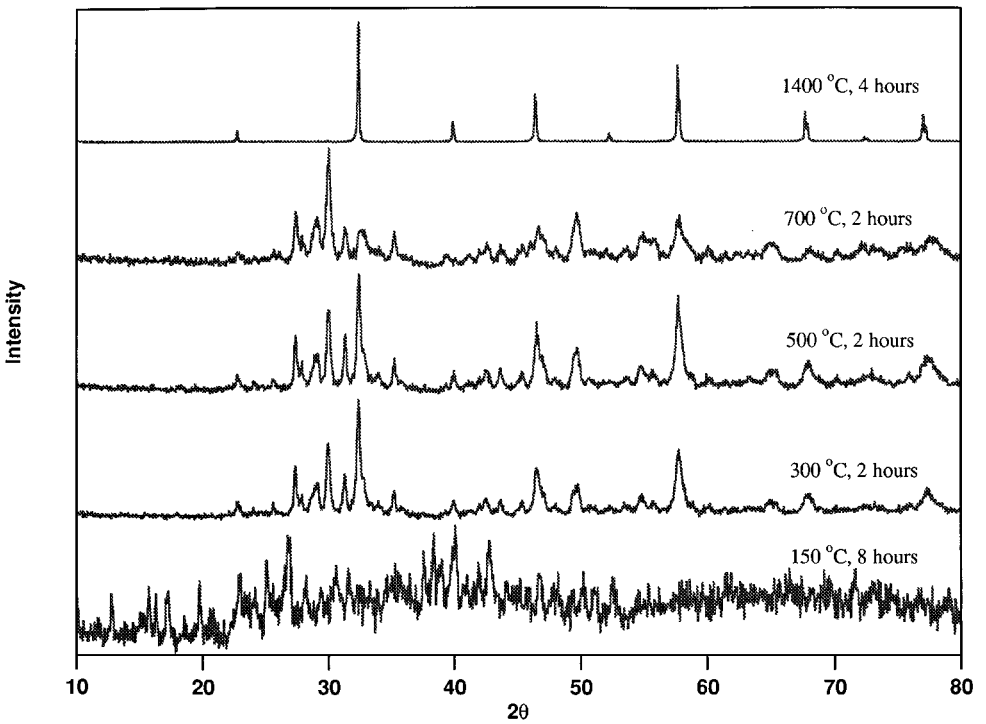

FIG. 1. Thermal evolution of the powder X-ray diffraction patterns of an LSGM sol–gel powder.

Hydrothermal treatment, like the Pechini method, not discussed in this study, is a well-developed routine to make ultrafine, agglomerate-free, multicomponent oxide powders. The principle of the hydrothermal reaction is based on an aqueous dissolution–precipitation process under high temperature and high pressure. The process can be briefly expressed by

$$A(\mathrm{OH})_s + B(\mathrm{OH})_s \xrightarrow{\text{dissolution}} A(\mathrm{OH})_{aq} + B(\mathrm{OH})_{aq} \xrightarrow{\text{precipitation}} ABO_3. \quad [3]$$

As already discussed, the precursor used for hydrothermal treatment is a complex containing aquo, hydroxo, and monocarboxylic ligands. It is difficult to predict whether the gel is dissolved under hydrothermal conditions as the solubility of such a gel is not available. XRD patterns of the hydrothermalized products did not reveal any difference from those before hydrothermal treatment; only amorphous phases were obtained. The final sintered products comprise mainly the cubic perovskite phase with a noticeable $LaSrGa_3O_7$ impurity. This result may imply a nonsimultaneous precipitation during the hydrothermal reaction, which causes an incorrect composition falling into the $LaSrGa_3O_7$ + P-cubic region of the phase diagram shown in ref 6.

3.2. Thermal Analysis

The DTA/TGA curves of the sol–gel-derived precursor after drying at 150°C are presented in Fig. 2a. The DTA curve exhibits a weak endothermic peak around 110°C, two stronger endothermic peaks at 220 and 280°C, respectively, a very strong exothermic peak starting around 330°C, and a weak exothermic peak around 360°C. The TGA curve shows weight changes corresponding to these peaks. Clearly, the first weak endothermic peak may be ascribed to the desorption of absorbed water. The subsequent stronger endothermic peak at 220°C must signal the loss of hydroxo ligands from $La(OH)_2(CH_3COO)$ to form $La(CH_3COO)_3$. The further decomposition of $La(CH_3COO)_3$ leads to the third endothermic peak at 280°C; the breakup of the bonds in the CH_3COO^- ligands releases great amounts of CH_4, CO, and H_2, which results in a substantial weight loss as indicated in the TGA curve (Fig. 2b). Breakup of the CH_3COO^- ligands is followed by a strong oxidation exothermic peak around 330°C and a weak exothermic peak around 360°C; no weight change is associated with the oxidation. The endo- and exothermic peaks couple around 300°C, which indicates final cleavage of the CH_3 and COO^- bonds left in CH_3COO^- and oxidation of the evolved gases, and this coupling appears to be a characteristic phenomenon for this precursor.

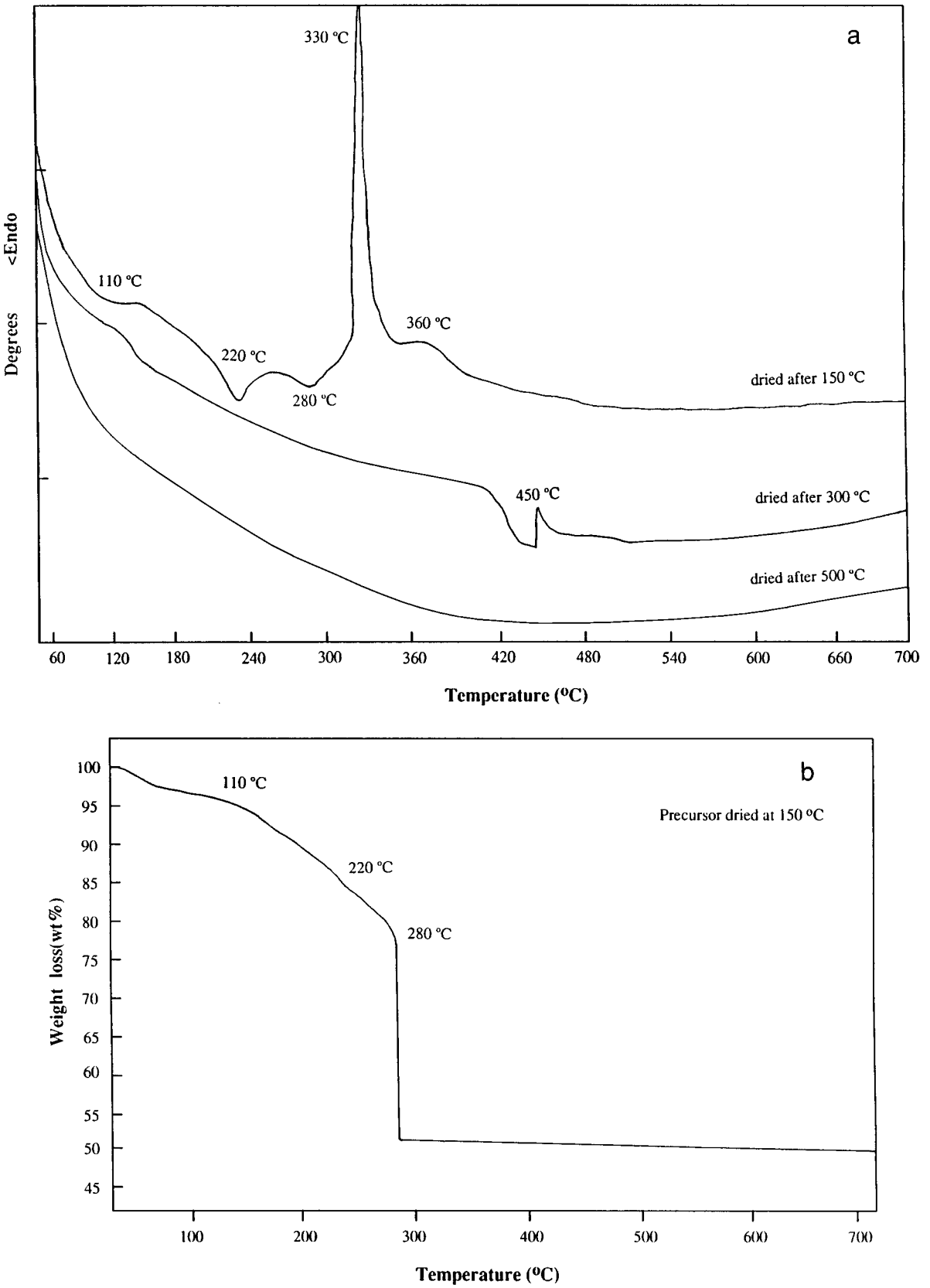

FIG. 2. Thermal analysis of the precursor and intermediate products derived from the sol–gel process: (a) DTA; (b) TGA.

As shown in Fig. 1, the intermediate product is multiphase; it contains La_2O_3, $LaSrGa_3O_7$, and $La_2O_2CO_3$ in addition to the main perovskite phase. Independent studies (13) support $La_2O_2CO_3$ as an intermediate product of the decomposition of $La(CH_3COO)_3$, and traces of $La_2O_2CO_3$ were found in the product even after heating to 700°C. The exothermic peak at 330°C occurs without any weight change, which we interpret to be due to an oxidation of the gaseous acetate ligands as they escape from the solid. The second, weak peak at 360°C may signal crystallization of the amorphous product.

In the case of $La(OH)_2(CH_3COO)$, the overall chemical reaction with increasing temperature can be illustrated as

$$La(OH)_2(CH_3COO) \xrightarrow{220^\circ C} La(CH_3COO) \xrightarrow{280^\circ C} La_2O_2CO_3 \xrightarrow{\text{exothermic induced}} La_2O_3. \quad [4]$$

For comparison, the DTA curves of the precursor after calcining at 300 and 500°C, respectively, are also shown in Fig. 2a. The associated endo- and exothermic peak couple at 450°C only occurred in the case of 300°C calcination. At 300°C, the hydroxo ligands are lost and the CH_3COO^- ligands should be broken down to give $La_2O_2CO_3$; the exothermic-induced breakup of $La_2O_2CO_3$ would not be initiated. The loss of the lower temperature endothermic peaks is therefore to be expected, but the shift of the exothermic peaks implies that a reaction between the $La_2O_2CO_3$ species has taken place at 350°C. A further rise of the calcination temperature to 500°C completes the decomposition of all components involved in this study, and no more peaks are observed.

The DTA curves of the hydrothermalized products (Fig. 3) similarly illustrate two endothermic peaks located around 100 and 280°C and a subsequent exothermic peak around 330°C, but they exhibit a very obscure endothermic shoulder located around 220°C that is different from the peak in Fig. 2a. Since this peak is associated with the hydroxo ligands, the change may imply some dissolution of the hydroxides into the aqueous solution when hydrothermalized. The fact that hydrothermalized powders are unable to form a single perovskite phase, as discussed in the

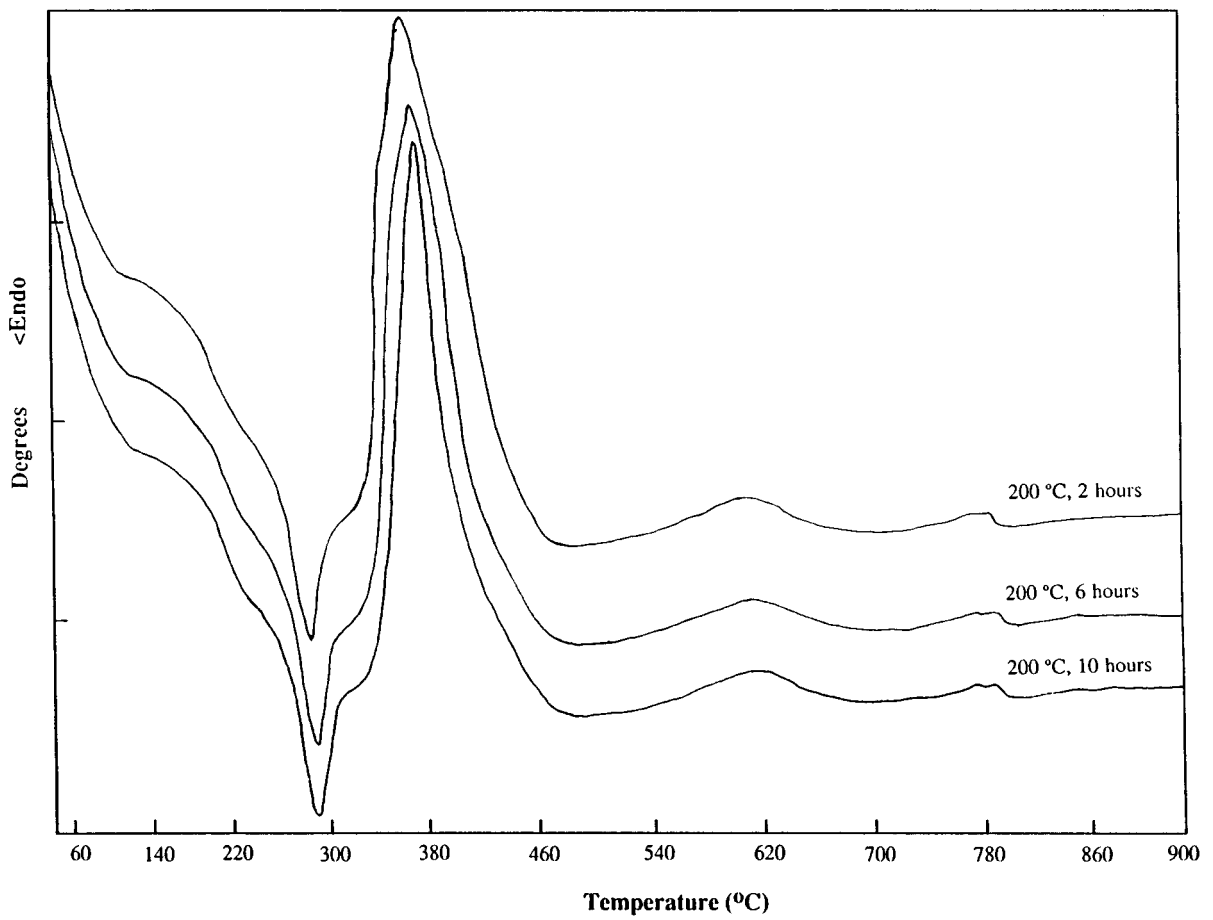

FIG. 3. DTA curves of the products derived from the hydrothermal process.

previous section, may also imply the precipitation of an incorrect composition. The two weak exothermic peaks around 600 and 800°C are due to the evolution of ethylene, which is produced by absorption of alcohol at the particle surfaces due to the hydrogen bonding of hydroxyl ions after subsequent alcohol washing. These two peaks are also accompanied by a gradual weight loss in the TGA curves.

3.3. IR Results

The as-synthesized precursor and calcined powders were investigated by IR spectroscopy. The IR spectrum of the gel after 150°C drying (Fig. 4a) exhibits extensive absorption peaks. The bands at 3383 and 3210 cm^{-1} are attributable to the bonded OH^- group; they are followed by weak bands at 2800 and 3000 cm^{-1} that are enhanced by heating (Figs. 4b–d) and can be ascribed to bonded OH^- in carboxylic acid. Other strong bands, produced by COO^- and C=O stretching vibrations (CH_3COO^- free ligand), were also observed at 1637 (CH_3COO^- free ligand), 1545 ($\nu_{as}COO^-$), and 1459 cm^{-1} (ν_s COO^-). They are followed by CH_3 bending vibrations, both of which occur between 1400 and 1350 cm^{-1}; CH_3 rocking vibrations were recorded at 1051 and 1036 cm^{-1} whereas the C–C stretching vibrations are positioned at 949 cm^{-1}. The band at 838 cm^{-1} may give an indication of an oxycarbonate phase having a bending vibration of ionic CO_3^{2-}. For wave numbers lower than 700 cm^{-1}, strong intensities of the fundamental bending vibrations of monocarboxylic acid groups like RCOOH (O–C=O; COO) appear at 658 and 614 cm^{-1}, respectively. Moreover, there are still several peaks, located at 2400, 817, and 741 cm^{-1}, that we are unable to identify as reasonable groups. These unidentified peaks possibly result from other anionic groups induced by the impurities.

After heating, the IR spectra exhibit significant changes in the OH^- and COO^- bands, but little change in the monocarboxylic acid bands. After an increase in temperature to 300°C (Fig. 4b), the broad OH^- and COO^- bands shown in Fig. 4a were greatly reduced, which implies a cleavage of the hydroxo and COO^- ligands. This observation confirms the related discussion in Section 3.2 very well. The vanishing of the CH_3 rocking vibration bands at 1051 and 1036 cm^{-1} after heating signals a gas release is involved. Further increases of temperature to 500 and 700°C lead to little change, which indicates a complete decomposition has occurred.

The IR spectra of the products of the 200°C hydrothermalized gel made from acetate salts are almost the same as those just described. No additional bands or changed positions were found. The only difference appears to be a sharper absorption at the OH^- and COO^- bands.

3.4. Powder Properties and Sintering

Figure 5 shows TEM micrographs of powders produced via (a) the sol–gel by ammonia peptization followed by calcination at 500°C for 2 hr, (b) hydrothermal treatment at 200°C for 6 hr, and (c) the Pechini method, calcined at 1000°C for 8 hr followed by ball-milling for 6 hr. The sol–gel-derived powders clearly exhibit well-crystallized particles with a size averaging 50 nm, but agglomerated together, probably due to the partial sintering when the exothermic reactions occurred. BET measurement gives a surface area of 5 m^2/g, as shown in Table 2. However, hydrothermalized powders, as shown in Fig. 5b, did not present any crystallization, but rather an amorphous phase, despite its high BET surface area. This observation may question the validity of a hydrothermal treatment for doped

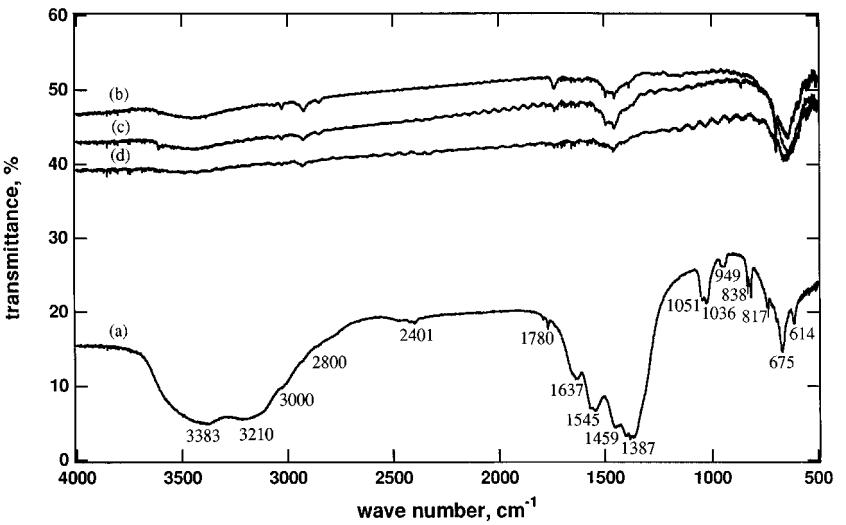

FIG. 4. IR spectra of the precursor and intermediate products derived from the sol–gel process: (a) 150°C; (b) 300°C; (c) 500°C; (d) 700°C.

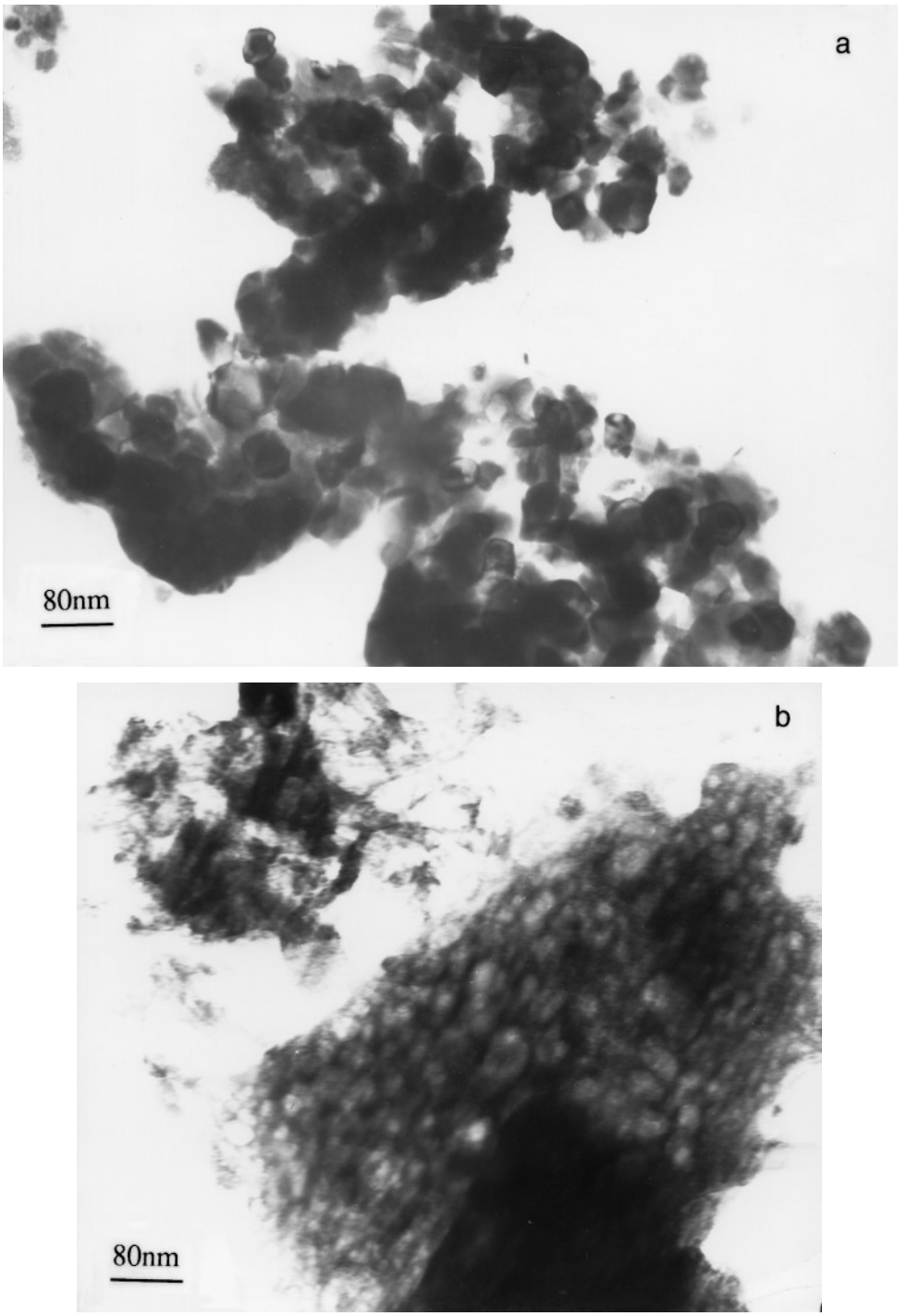

FIG. 5. TEM micrographs of an LSGM powder derived by different routes: (a) sol–gel; (b) hydrothermal treatment; (c) Pechini method.

TABLE 2
Powder Properties Derived by Different Methods

	Particle size (nm)	BET surface area (m^2/g)	Density after 6 hr of sintering at 1400°C (g/cm^3)	Phases existing after 6 hr of sintering at 1400°C
Sol–gel	50	5.0	6.18	P-cubic
Hydrothermal	10	92.0	5.19	Cubic + $LaSrGa_3O_7$
Pechini	150	4.5	6.34	P-cubic

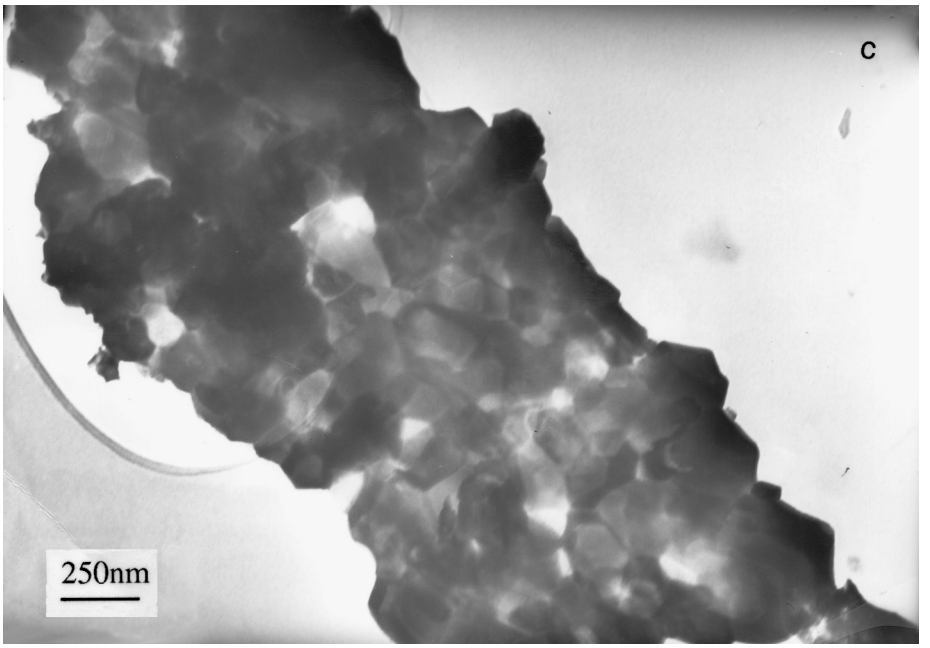

FIG. 5—*Continued*

$LaGaO_3$ perovskite, and a more detailed investigation needs to be carried out.

Table 2 also indicates that sol–gel-derived and Pechini powders are not only easily sintered to a dense ceramic body but also formed into a single perovskite cubic phase, which has already been identified in this composition (5).

4. CONCLUSIONS

LSGM electrolyte can be prepared as a single-phase cubic perovskite by both the sol–gel process and the Pechini method, but not by hydrothermal treatment. The high coordination numbers of the cations and smaller electronegativity of CH_3COO^- lead to a homogeneous gel with a strong complexation between cations and anions under basic conditions, which contain OH^- and CH_3COO^- ligands. DTA/TGA measurements reveal corresponding endothermic peaks at 220 and 280°C, respectively, for the cleavage of OH^- and CH_3COO^- bonds with the liberation of evolved gases and a following strong exothermic peak at 330°C. The coupling of the endothermic peak at 280°C and the exothermic peak at 330°C is a characteristic phenomenon for the cleavage of the CH_3COO^- ligands. IR spectroscopy further confirms the existence of OH^- and CH_3COO^- ligands in the dried gel and their gradual disappearance with increasing temperature. The powders thus obtained, as indicated by TEM and BET, exhibit an average particle size of 50 nm with a surface area of 5 m^2/g. On the other hand, hydrothermal treatment of the gel did not produce well-crystallized powders with correct compositions, but these powders have a higher BET surface area. Further work is needed to clarify the dissolution–precipitation process involved in the hydrothermal treatment.

ACKNOWLEDGMENT

We thank the Electric Power Research Institute (EPRI) for financial support (Contract 8062-08). Dr. Wate Bakker is the manager of the project.

REFERENCES

1. T. Ishihara, H. Matsuda, and Y. Takita, *J. Am. Chem. Soc.* **116,** 3801 (1994).
2. M. Feng and J. B. Goodenough, *Eur. J. Solid State Inorg. Chem.* **T31,** 663 (1994).
3. K. Q. Huang, M. Feng, and J. B. Goodenough, *J. Am. Ceram. Soc.* **79,** 1100 (1996).
4. K. Q. Huang, M. Feng, J. B. Goodenough, and M. Schmerling, *J. Electrochem. Soc.* **143,** 3630 (1996).
5. K. Q. Huang, R. Tichy, and J. B. Goodenough, *J. Am. Ceram. Soc.*, in press.
6. K. Q. Huang, R. Tichy, and J. B. Goodenough, *J. Am. Ceram. Soc.*, in press.
7. K. Q. Huang, R. Tichy, and J. B. Goodenough, *J. Am. Ceram. Soc.*, in press.
8. G. W. Morey, *J. Am. Ceram. Soc.* **36,** 279 (1953).
9. W. J. Dawson, *Ceramic Bull.* **67**(10) (1988).
10. J.-D. Lin and J.-G. Duh, *J. Am. Ceram. Soc.* **80,** 92 (1997).
11. M. Pechini, U.S. Patent 3 330 697, July 11, 1967.
12. P. A. Lessing, *Ceramic Bull.* **68**(5) (1989).
13. L. W. Tai and P. A. Lessing, *J. Mater. Res.* **7,** 502, 511 (1992).

14. N. G. Eror and H. U. Anderson, *in* "Better Ceramics through Chemistry II, Materials Research Society Symposia Proceedings" (C. J. Brinker, D. E. Clark, and D. R. Ulrich, Eds.), Vol. 73, pp. 571–577. Materials Research Society, Pittsburgh, PA, 1986.
15. E. Matijevic, *Annu. Rev. Mater. Sci.* **15,** 483 (1985).
16. R. S. Sapiezsko, R. C. Patel, and E. Matijevic, *J. Phys. Chem.* **81,** 1069 (1977).
17. V. Strahm, R. C. Patel, and E. Matijevic, *J. Phys. Chem.* **83,** 1689 (1979).
18. P. H. Fries, N. R. Jagannathan, F. G. Herring, and G. N. Patey, *J. Phys. Chem.* **91,** 215 (1987).
19. A. Fratiello, "Inorganic Chemical Reaction Mechanisms, Part II" (J. O. Edwards, Ed.), p. 57. Interscience, New York, 1972.
20. M. Magini and R. Caminiti, *J. Inorg. Nucl. Chem.* **39,** 91 (1977).
21. M. Magini, *J. Inorg. Nucl. Chem.* **40,** 43 (1978).